Talanta 116 (2013) 726–735

Contents lists available at ScienceDirect

Talanta

journal homepage: www.elsevier.com/locate/talanta

Sol–gel thin-film based mesoporous silica and carbon nanotubes for the determination of dopamine, uric acid and paracetamol in urine

Thiago C. Canevari [a,*], Paulo A. Raymundo-Pereira [a], Richard Landers [b], Edilson V Benvenutti [c], Sérgio A.S. Machado [a]

[a] Institute of Chemistry, State University of São Paulo, PO Box 780, 13560-970 São Carlos, SP, Brazil
[b] Institute of Chemistry, Federal University of Rio Grande do Sul, Porto Alegre, RS, Brazil
[c] Institute of Physics Gleb Wataghin, State University of Campinas, Campinas, SP, Brazil

ARTICLE INFO

Article history:
Received 9 April 2013
Received in revised form
17 July 2013
Accepted 19 July 2013
Available online 31 July 2013

Keywords:
Carbon nanotubes
Mesoporous silica
Electrochemical sensor
Dopamine
Uric acid
Paracetamol

ABSTRACT

This work describes the preparation, characterization and application of a hybrid material composed of disordered mesoporous silica (SiO_2) modified with multiwalled carbon nanotubes (MWCNTs), obtained by the sol–gel process using HF as the catalyst. This hybrid material was characterized by N_2 adsorption–desorption isotherms, X-ray powder diffraction (XRD), scanning electron microscopy (SEM), high resolution transmission microscopy (HR-TEM), Raman spectroscopy and X-ray photoelectron spectroscopy (XPS). This new hybrid material was used for the construction of a thin film on a glassy carbon electrode. The modified electrode using this material was designated SiO_2/MWCNT/GCE. The electrocatalytic properties of the electrode toward dopamine, uric acid and paracetamol oxidation were studied by differential pulse voltammetry. Well-defined and separated oxidation peaks were observed in phosphate buffer solution at pH 7.0, in contrast with the ill-defined peaks observed with unmodified glassy carbon electrodes. The electrode had high sensitivity for the determination of dopamine, uric acid and paracetamol, with the limits of detection obtained using statistical methods, at 0.014, 0.068 and 0.098 μmol L^{-1}, respectively. The electrode presented some important advantages, including enhanced physical rigidity, surface renewability by polishing and high sensitivity, allowing the simultaneous determination of these three analytes in a human urine sample.

1. Introduction

Carbon-based materials, mainly carbon nanotubes, have attracted much interest in the development of electrodes to be used in electroanalytical chemistry. Carbon nanotubes (CNTs) have a hexagonal structure of carbon atoms similar to the atomic planes of the graphite structure, with conjugated bonds and carbon atoms on a trigonal planar geometry. These materials have, as their main features, a high surface area, mechanical strength, biocompatibility, excellent electrical conductivity, and high chemical stability; as such, they have been widely used in the development of electrochemical sensors [1–5]. Modified electrodes, which are defined by changes to a solid surface electrode by immobilizing different substances (molecules, polymers, carbon nanotubes, etc.), usually have greater sensitivity and selectivity when compared to non-modified ones. Modified electrodes have defined a very attractive research area in electroanalysis due to their widespread application in numerous analytical methodologies [6]. Among the various types of electrode modifiers, materials based on silica (SiO_2) obtained by the sol–gel process appear to be an excellent choice for electrode modification in the development of chemical sensors [7,8]. These materials have characteristics such as a high surface area, high porosity, mechanical strength, high chemical and thermal stability and a reactive surface as a function of silanol groups (Si–OH), facilitating further immobilization of other species [9,10]. According to IUPAC [11], silica can be classified as microporous, mesoporous and macroporous according to the size and distribution of pores. Mesoporous silica, with pore diameters ranging from 2 to 50 nm, shows enhanced interactions with different external reagents and fast mass transfer rates of the analyte inside the porous structure [12,13], which provide a high sensitivity to the sensor device. A very interesting application of mesoporous silica, that has become an attractive research field, is related to the immobilization of carbon nanotubes on mesoporous silica. Carbon nanotubes can be incorporated into the silica matrix in several ways, e.g. mesoporous silica film on an SWCNT film [14], post-functionalization of a silica matrix by covalent bonding of the carboxyl groups of CNTs [15], post-functionalization by a CVD procedure with CNTs [16] and MWCNTs grafted onto the silica network [17]. These modifications are

* Corresponding author. Tel./fax: +55 16 3521 3109.
E-mail address: tccanevari@gmail.com (T.C. Canevari).

0039-9140/$ - see front matter Crown Copyright © 2013 Published by Elsevier B.V. All rights reserved.
http://dx.doi.org/10.1016/j.talanta.2013.07.044

performed in order to reduce the electrical resistance of the silica matrix and increase the electrocatalytic properties of the surface, thus facilitating the transference of electrons at low overpotentials [18]. In previous studies, the mesoporous silica matrix was prepared using templating methods. In this work, the matrix of mesoporous silica was obtained using HF as the catalyst without using templates, in which carbon nanotubes were physically incorporated into the silica matrix and did not participate in any chemical reactions during the formation of mesoporous silica.

Dopamine (DA) and uric acid (UA) are biologically important compounds in human metabolism. DA is an important neurotransmitter molecule and it plays vital roles in the function of the central nervous, renal, hormonal and cardiovascular systems. Low levels of DA are related to neurological disorders such as Parkinson ′s disease [19], schizophrenia [20,21] and HIV infection [22]. Uric acid (UA) is the primary end product of purine metabolism. Abnormal levels of UA are symptoms of several diseases, such as hyperuricemia, gout, Lesch–Nyhan syndrome, obesity, diabetes, high cholesterol and high blood pressure [23,24]. Hence, monitoring the concentration of UA in biological fluids is indispensable for the diagnosis of patients suffering from several disorders.

Paracetamol (PAR) (acetaminophen, *N*-acetyl-*p*-aminophenol) is a popular active ingredient in the pharmaceutical industry and is widely used as an antipyretic medicament. It is normally preferred for patients with problems with acetylsalicylic acid (e.g., aspirin). Generally, paracetamol does not induce any harmful side effects, however, hypersensitivity or overdoses of paracetamol lead to hepatotoxicity and nephrotoxicity and can also cause pancreatic diseases [25,26]. The oxidation process of these compounds is very important in the living body.

Many analytical methods for the determination of DA, UA and PAR in biological fluids have been employed, such as chromatography [27–29], spectrophotometric [30,31], fluorescence [32–34] and electrochemical methods [35,36]. The electrochemical system is one of the most commonly used techniques in environmental and biological research because of its high sensitivity, rapid response, low detection limit and easy operation. Electrochemical methods have been proposed for the development of a simple procedure to determine DA, UA and PAR at the so-called "point-of-care" with a fast methodology. However, the electrochemical oxidation of DA, UA and PAR on a surface of unmodified or bare electrodes takes place only at high overpotentials without separation between their oxidation peaks [37,38] and causes fouling of the electrode surface. Therefore, it is necessary to develop an effective electrochemical sensor for the detection of these biological compounds in a real sample. By combining the advantages of the sol–gel process with the ability of MWCNTs to mediate the electron transfer reaction, in this work, a new hybrid material was developed and applied as a film on glassy carbon electrodes used for sensitive dopamine, uric acid and paracetamol detection.

2. Experimental

2.1. Reagents

All the reagents used in this work were of analytical grade purity: tetraethyl orthosilicate, TEOS (Sigma–Aldrich, 98%); multi-wall carbon nanotubes (MWCNT, diameter: 110–170 nm, Sigma–Aldrich, 99.9%), ascorbic acid (Aldrich), dopamine (Sigma), uric acid (Aldrich) and paracetamol. Other reagents used were: ethanol (Sigma–Aldrich 99.9%) and HF (Synth, 47%). Phosphate buffer solution (PBS, 0.1 mol L^{-1}, pH 7.0) was prepared from NaH_2PO_4 and Na_2HPO_4. All aqueous solutions were prepared with ultrapure water obtained from a Milli-Q Plus system (Millipore). A human urine sample was provided by a healthy volunteer.

2.2. Synthesis of disordered mesoporous silica containing 10 wt% carbon nanotubes (SiO_2/MWCNT)

The preparation of a mesoporous silica sample containing 10 wt% carbon nanotubes (SiO_2/MWCNT) was synthesized according to the following procedure. First, a suspension was prepared by mixing TEOS (0.045 mol) and ethanol 1/1 (v/v) and stirring for 20 min. Then, 4 mL of H_2O were added, maintaining the proportion of Si/H_2O (1:4), together with 0.9 g of multi-walled carbon nanotubes, and the suspension was ultrasonicated for 20 min. To the resulting mixture, 0.3 mL of HF (48%) was added under sonication until gel formation was observed. The obtained gel was stored for up to 7 days at room temperature. The xerogel was ground and the powder was washed with ethanol in a Soxhlet extractor for 2 h and subsequently submitted to a heat treatment at 323 K to evaporate all residual solvent.

2.3. Functionalization of SiO_2/MWCNT with an acid mixture

The oxidation of the carbon nanotubes physically incorporated into the mesoporous silica matrix was carried out by the dispersion of the hybrid material in a mixture of sulfuric acid and nitric acid, according to the following procedure. The mixture consisted of 1.0 g SiO_2/MWCNT (as prepared) in 200 mL of a 1:3 volume of concentrated HNO_3/H_2SO_4 solution. The resulting mixture was kept under magnetic stirring at room temperature for 12 h and was subsequently filtered through a 0.45-μm Millipore nylon filter membrane. The resulting material (treated) was continuously washed using purified water until the pH of the filtrate was neutral, and then it was dried for 3 h in a vacuum oven at 373 K. The obtained material was designated SiO_2/MWCNT/func.

This functionalization aimed to promote the formation of hydroxyl groups (–OH), carboxyl (–COOH), anhydride and esters ($-COO^-$) on the surface of the carbon nanotubes physically incorporated into the mesoporous silica matrix [39]. Another effect caused by acid treatment was an increase in the available surface area due to the opening and rupture of the cylindrical nanotubes by weakening of the Van der Waals forces, providing increased surface area of the material.

2.4. Preparation of an SiO_2/MWCNT film on a glassy carbon electrode surface (SiO_2/MWCNT/GCE)

The working electrode was prepared by modifying the surface of the glassy carbon electrode (GC). On the electrode surface, a thin film of the SiO_2/MWCNT/func material was prepared according to the following procedure. Previously, a solution was prepared by mixing 50 mg of the SiO_2/MWCNT/func material, 10 mL of H_2O and 20 μL of 5% Nafion solution, which was then subjected to 10 min of ultrasonication. Then, a 9 μL drop was added to the surface of the glassy carbon electrode with a geometric area of 0.07 cm^2. To complete film formation, the electrode was left under flowing nitrogen for 10 min. The electrode was prepared by forming a thin film material of SiO_2/MWCNT/func on the surface of the glassy carbon, which was designated SiO_2/MWCNT/func/GCE. In addition, a film was prepared on a GC electrode with the SiO_2/MWCNT material without functionalization, which was designated SiO_2/MWCNT/GCE.

2.5. Apparatus

The Brunauer – Emmett – Teller (BET) method was employed to calculate the specific surface areas (S_{BET}), and the BJH method was employed to study the pore distribution of the SiO_2/MWCNT hybrid material. N_2 adsorption – desorption isotherms were measured at

77 K on a Micromeritics Tristar Kripton instrument. Samples were previously outgassed at 400 K for 10 h.

X-ray powder diffraction (XRD) analysis was performed on a Rigaku Rotoflex RU 200B diffractometer equipped with Cu $K\alpha$ radiation ($\lambda = 1.54178$ Å) operating in continuous scan mode at 2° min^{-1}. The measurements were collected at room temperature with a scan range between 3° and 60°.

The morphologies of the SiO_2/MWCNT/func were examined by means of a field emission gun by scanning electron microscopy (FEG-SEM) using a FEG-Zeiss model Supra 35VP (Zeiss, Germany) equipped with a high-resolution secondary electron detector (in-lens detector), operating at 6.0 kV and a point-to-point resolution of 3.8 nm.

High-resolution transmission electron microscopy (HRTEM) images were obtained on a FEI TECNAI G² F20 transmission electron microscope operating at 200 kV. The powders were ultrasonically suspended in ethanol for 30 min, and the suspension was deposited on carbon-coated copper grids.

Pristine and functionalized SiO_2/MWCNT/func were characterized by Raman spectroscopy. Spectra were recorded using the 514.5 nm line of a helium–neon laser at a power of 150 W and spectral resolution of 1 cm^{-1}.

The X-ray photoelectron spectrum (XPS) of the SiO_2/MWCNT/func was obtained from a VSW HA 100 hemispherical electron analyzer, using an Al anode as the X-ray source. The X-ray source was operated at 12 keV and 15 mA. The correction of the binding energies for charge was obtained using the reference Si2p line from silica, which was set at 103.4 eV [40].

Electrochemical measurements were performed on a PGSTAT-20 galvanostat–potentiostat using an electrochemical cell composed of a working electrode (SiO_2/MWCNT/func/GCE), reference electrode (Ag/AgCl) and counter electrode (Pt). The electrochemical techniques used were cyclic voltammetry and differential pulse voltammetry. Measurements were made in an electrochemical cell containing 20 mL of PBS supporting an electrolyte solution with a scan rate of 10 mV s^{-1}.

3. Results and discussion

3.1. Structural characterization

Fig. 1 shows (a) the adsorption and desorption isotherms of N_2 and (b) the graph of the pore size distribution for the SiO_2/MWCNT hybrid materials and pure silica (SMD). According to Fig. 1a, all materials exhibited type IV isotherms and the presence of hysteresis in regions of relatively high pressure ($P/P_0 > 0.7$), a feature of mesoporous materials [11,41,42]. The disordered mesoporous structure presented by SiO_2/MWCNT hybrid materials was due to the HF acid catalyst [43]. The hysteresis presented by all materials was of type H2, characteristic of disordered materials with a heterogeneous pore distribution [44]. The heterogeneous distribution of the pores was confirmed by the results shown in Fig. 1b, where the materials exhibit average pore sizes ranging from 10 to 13 nm. Table 1 shows the values of surface area (S_{BET}) and pore volume (P_V) for SiO_2/MWCNT/func, SiO_2/MWCNT and of silica (SMD).

Table 1 shows a significant increase in the value of surface area and pore volume of the SiO_2/MWCNT hybrid materials over silica. This increase was expected because the carbon nanotubes were incorporated into the mesoporous silica matrix [45], as shown by the FEG-SEM and HR-TEM images (Figs. 3 and 4, respectively). The increase in pore volume between SiO_2/MWCNT/func and SiO_2/MWCNT was due to acid treatment of the material. This acid treatment increased the surface area available through the opening and rupture of cylindrical nanotubes by weakening the Van der Waals forces, providing increased surface area to the material [46,47].

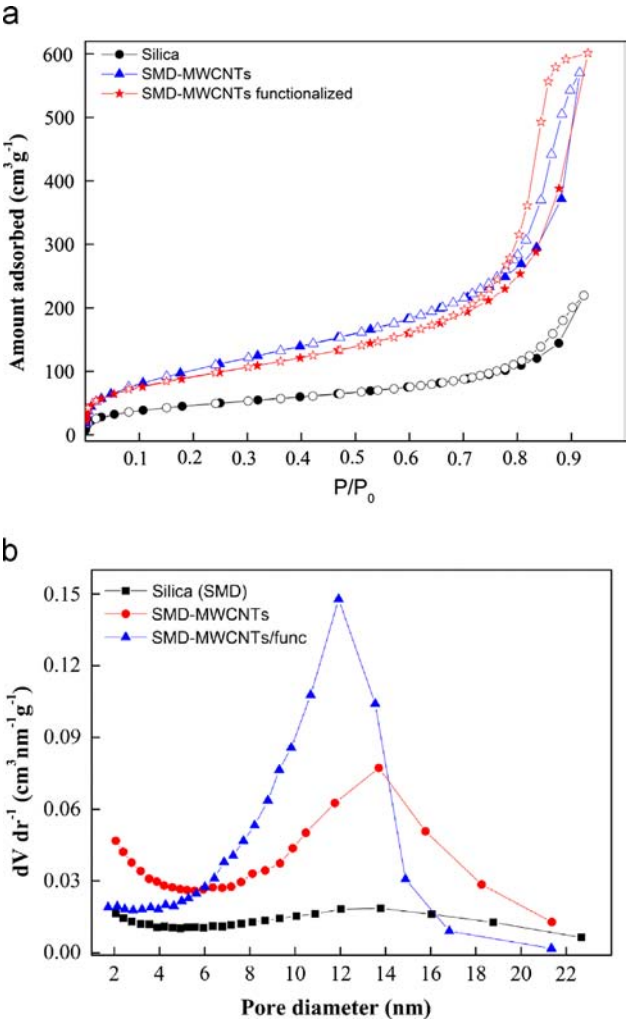

Fig. 1. (a) Nitrogen adsorption–desorption isotherms and (b) BJH pore size distribution curve of SiO_2/MWCNT/func, SiO_2/MWCNT and SiO_2 materials.

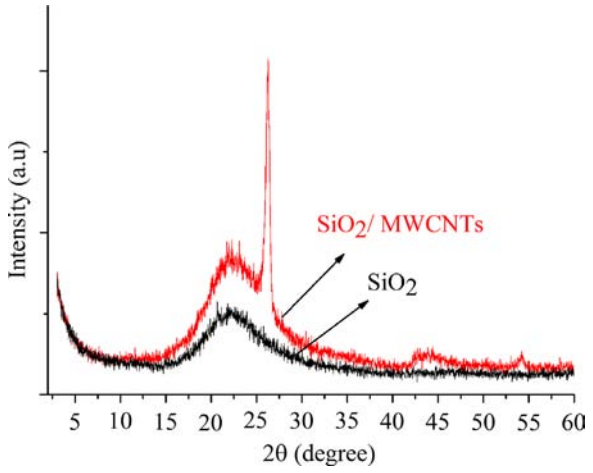

Fig. 2. XRD spectrum of mesoporous silica (SiO_2) and the SiO_2/MWCNT/func hybrid material.

The increase in pore volume confirmed the mesoporosity of the hybrid material and facilitated mass transfer rates of the analyte by the porous structure.

In addition, to demonstrate that the hybrid material had a disordered structure, the XRD patterns of the SiO_2/MWCNT/func hybrid material and silica (SMD) were obtained (Fig. 2). As can

Table 1
Values of surface area (S_{BET}) and pore volume (P_V) of the SiO_2/MWCNT/func, SiO_2/MWCNT and SiO_2 materials.

Sample	S_{BET} ($m^2\ g^{-1}$)	P_v ($cm^3\ g^{-1}$)
Silica (SiO_2)	168	0.3
SiO_2/MWCNTs	386	0.82
SiO_2/MWCNTs/func	333	0.91

Error: ± 10%.

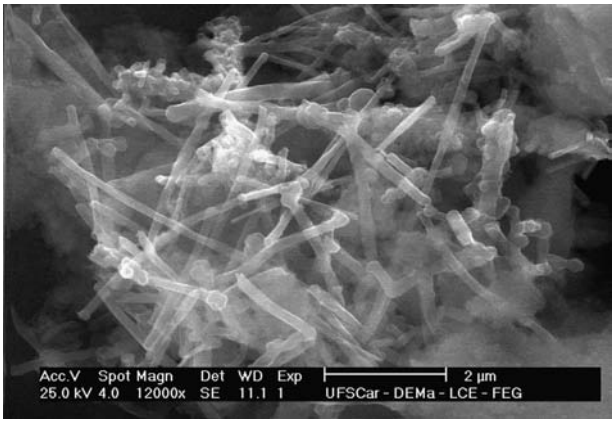

Fig. 3. SEM image of the SiO_2/MWCNT/func material.

been seen, both the hybrid material and silica presented an amorphous structure due the absence of peak reflection in the XRD diffractograms. Based on these results, it is possible to state that both materials did not have periodicity and were disordered. The diffraction peaks at 26–28° and 42.75° were assigned to the (0 0 2) and (1 0 0) planes of MWNCTs, respectively [48], showing the incorporation of MWCNTs in the disordered silica mesoporous matrix Fig. 2.

3.2. FEG-SEM images and HR-TEM micrographs

The FEG-SEM images of the SiO_2/MWCNT/func material, at a magnification of 12,000 ×, show that carbon nanotubes had various lengths and diameters and were dispersed throughout the silica framework (Fig. 3). This was confirmed through transmission electron microscopy (TEM) analysis. Fig. 4 shows high resolution transmission electron microscopy (HR-TEM) images of the SiO_2/MWCNT/func material. High magnification HRTEM images provided insights into the microstructure of the hybrid material by showing that the nanotubes were embedded within the mesoporous silica matrix (Fig. 4a). Fig. 4b shows that carbon nanotube structure was preserved, although some defective cylindrical graphene sheet structures appeared [49], after the carbon nanotubes were physically incorporated into the mesoporous silica matrix Figs. 3 and 4.

3.3. Raman spectra for the SiO_2/MWCNT hybrid material

Raman spectra provided important complementary data for the characterization of the nanotube structure in the SiO_2/MWCNT/func hybrid material by providing information about the microstructure of the materials. As can be seen in Fig. 5a, three peaks at ca. 1340.7, 1562 and 2676 cm^{-1} were observed. The band with a maximum near 1350 cm^{-1} is common in disordered trigonal planar carbon materials, and it has been called the D-band. It is activated by disorder in the trigonal carbon network in the presence of vacancies, grain boundaries or any defects. The band at 1562 cm^{-1} is close to that observed for well-ordered graphite (i.e., E_{2g} band at 1582 cm^{-1}), and it is often called the G-band [50,51]. The G-band in well-ordered

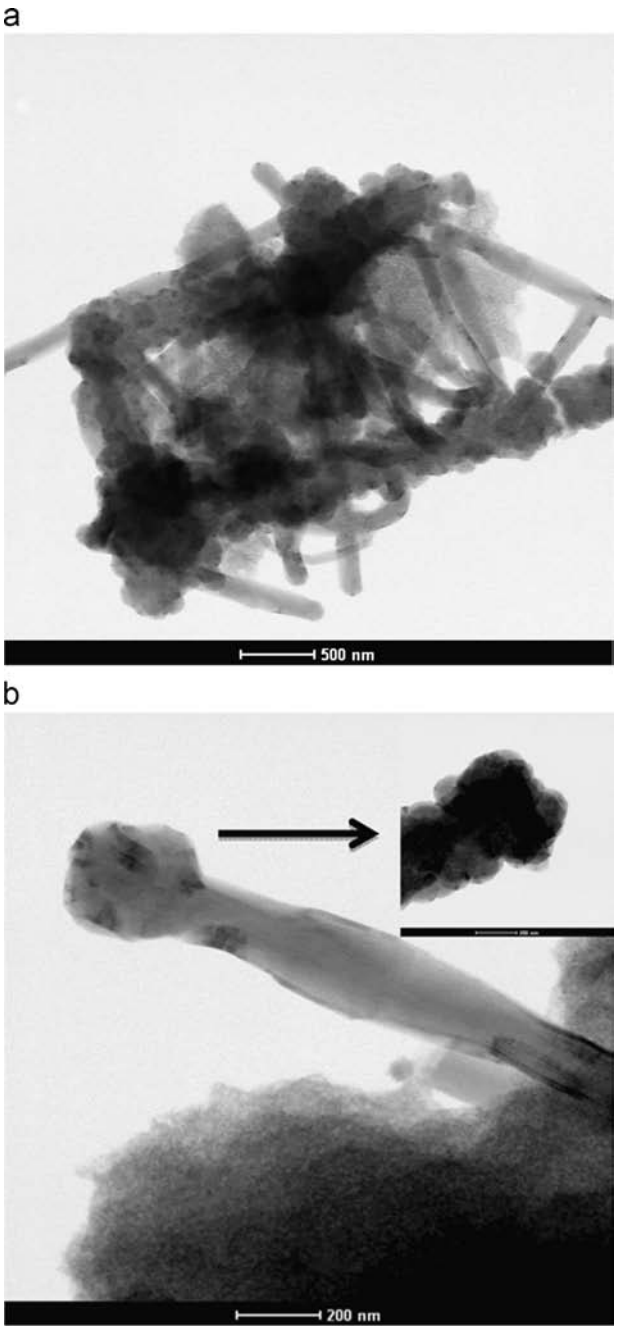

Fig. 4. HR-TEM micrographs of (a) SiO_2/MWCNT and (b) SiO_2/MWCNT/func.

nanotubes actually has several components that stem from the perfect cylindrical symmetry of the nanotube. In comparison with the SiO_2/MWCNT hybrid material without acid treatment (Fig. 5b), an intensity difference was observed in band D and in band G. These occurred because the acid treatment caused a partial destruction of MWCNTs and an increased the amount of disorganized carbon structures [52].

The band at 2676 cm^{-1} provides information about the electronic structure of carbon nanotubes embedded in the silica matrix and has been called the G′-band (D-band overtone) [53].

3.4. X-ray photoelectron spectroscopy (XPS)

X-ray photoelectron spectroscopy (XPS) analysis was performed in order to acquire information about the surface and the nature of the chemical bonds. Table 2 summarizes the XPS

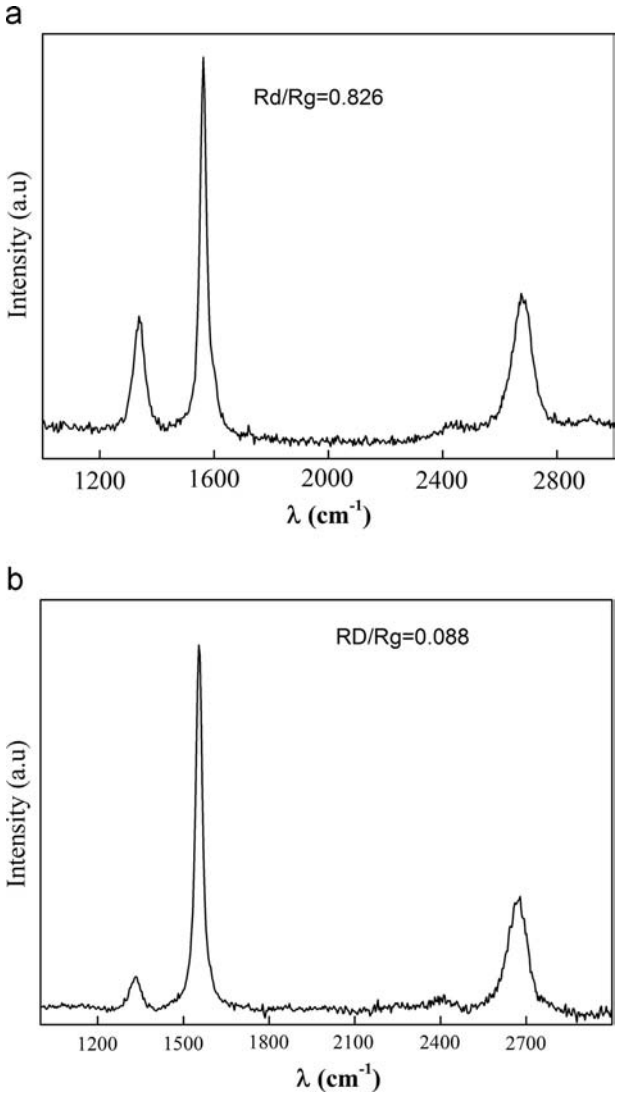

Fig. 5. Raman spectra of (a) SiO_2/MWCNT/func and (b) the SiO_2/MWCNT hybrid material.

Table 2
Summary of the XPS binding energy values (eV) obtained for SiO_2/MWCNT/func.

Sample	C1s					O1s	Si2p
SiO_2/MWCNTs/Func	284.7 (1.6) [52]	286.3 (2.2) [20]	288.6 (2.2) [10]	291.0 (2.2) [13]	292.9 (2.1) [5]	532.8 (3.0)	103.5 (3.0)

binding energy (eV) values of C1s, O1s and Si2p obtained for the SiO_2/MWCNT/func material.

The binding energy (B.E.) values of C1s at 284.7, 286.3, 288.6, 291 and 292.9 eV were assigned to carbon bonded atoms in polyaromatic structures in graphite (B.E.=284.6 eV), carbon present in alcohol, ether or C=N groups (B.E.=286.0–286.3 eV), carboxyl or ester groups (B.E.=288.8–289.1 eV), carbonate groups (B.E.=290.5–291.2 eV) and satellite peaks due to π–π^* transitions in aromatic rings (B.E.=291.6 eV) [54–57].

As a consequence, the binding energy value of O1s at 532.8 eV was assigned to carbonyl oxygen atoms in esters, anhydrides and oxygen atoms in hydroxyl groups [56]. This implies that the SiO_2/MWCNT/func material is ideal for efficient further chemical modifications.

3.5. Electrochemical measurements

Cyclic voltammetry was used to evaluate the electrochemical response of bare GC and SiO_2/MWCNT electrodes before and after

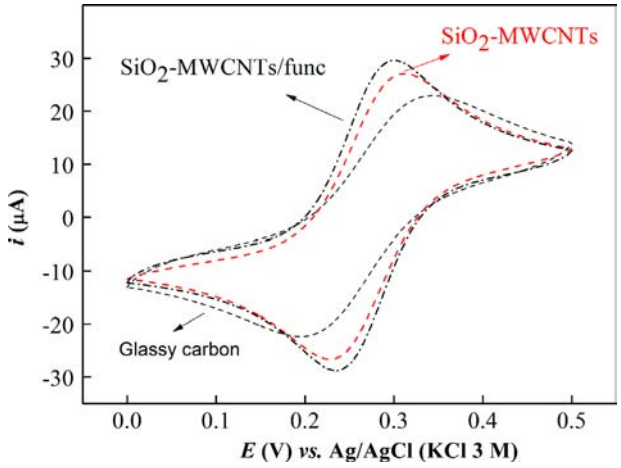

Fig. 6. Voltammetry cyclic profiles at three different electrodes (bare GC, SiO_2/MWCNT/GCE and treated SiO_2/MWCNT/func/GCE) in a 5 mmol L^{-1} $[Fe(CN)_6]^{3-/4-}$ redox couple solution.

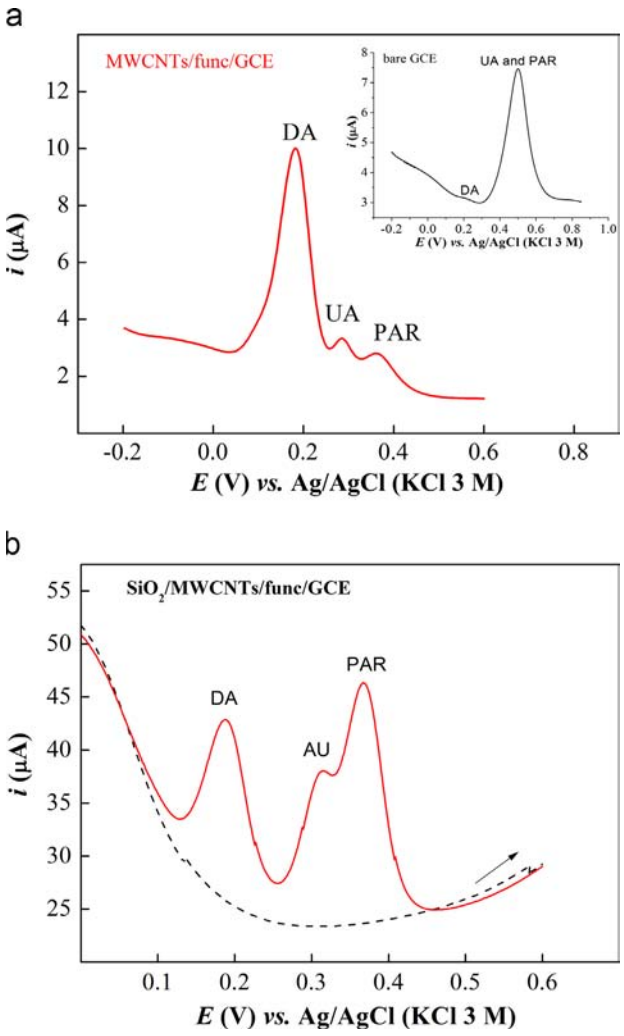

Fig. 7. Differential pulse voltammograms of dopamine (DA), uric acid (UA) and paracetamol (PAR): (a) MWCNT/func/GCE (inset figure bare GCE) and (b) SiO_2/MWCNT/func/GCE. Measurements performed with the same concentrations of 4.0×10^{-5} mol L^{-1} dopamine, uric acid and paracetamol in PBS, pH 7.0.

acid treatment. Fig. 6 shows the voltammetric profiles at three different electrodes (bare GC, SiO_2/MWCNT/GCE and SiO_2/MWCNT/func/GCE) in a 5 mmol L^{-1} $[Fe(CN)_6]^{3-/4-}$ redox couple solution. As can be seen, the SiO_2/MWCNT/func/GCE electrode exhibited well-defined peaks with a small peak of potential separation (ΔE) of 62 mV and increased peak current when compared with SiO_2/MWCNT/GCE (ΔE) of 77 mV and bare GC (ΔE) at 149 mV, indicating that MWCNTs facilitate/accelerate the transfer of electrons in the electrode surface. The enhanced electron transfer kinetics at the SiO_2/MWCNT/func/GCE electrode were attributed to an increase in the edge plane area available to the electroactive species, caused by the acid functionalization of MWCNTs, thereby increasing the electric conductivity on the electrode surface [49]. Since the best results were found with the SiO_2/MWCNT/func/GCE electrode prepared with the material subjected to acid treatment, this was used in the electrocatalytic study of dopamine, uric acid and paracetamol.

3.6. Electrochemical oxidation of dopamine, uric acid and paracetamol

The difference in the electrochemical behavior of the bare glassy carbon electrode (GCE), MWCNT/func/GCE and SiO_2/MWCNT/func/GCE electrodes in relation to dopamine, uric acid and paracetamol was initially examined via differential pulse voltammetry in PBS buffer, pH 7.0 with the analyte concentration fixed at 4×10^{-5} mol L^{-1}. Fig. 7 shows the determination of dopamine, uric acid and paracetamol by the MWCNT/func/GCE (a) and the SiO_2/MWCNT/func/GCE electrodes (b), respectively. As can be seen, the electrode modified with functionalized MWCNTs, (MWCNT/GCE) exhibited three well-defined and separate peaks for dopamine (E=0.182 V), uric acid (E=0.29 V) and paracetamol (E=0.36 V) (Fig. 7a), indicating that the MWCNT/func/GCE electrode exhibited electrocatalytic activity in relation to dopamine, uric acid and paracetamol. Similarly, when the determination was performed at the SiO_2/MWCNT/func/GCE electrode, there was also good peak separation for dopamine (DA, 0.18 V), uric acid (UA, 0.315 V) and paracetamol (PAR, 0.382 V), as shown in Fig. 7b. However, the SiO_2/MWCNT/func/GCE electrode showed a better electrocatalytic response in comparison the MWCNT/func/GCE electrode as it provided a greater increase in current for the same concentrations of dopamine, uric acid and paracetamol. With these results, we can suggest that the mesoporous silica matrix directs physically incorporated carbon nanotubes, leaving the extremities exposed for the reaction, as shown by SEM and TEM analysis. Therefore, the hybrid material, SiO_2/MWCNT/func, presents a better electrocatalytic response. The good peak separations and good electrocatalytic activity indicate that the SiO_2/MWCNT/func/GCE electrode can identify and separate dopamine, uric acid and paracetamol simultaneously.

The same test was performed using the bare glassy carbon electrode (inset Fig. 7a). A small peak at 0.2 V relative to dopamine oxidation and an overlapping oxidation peak at 0.5 V relative to a mixture of uric acid and paracetamol were observed. This indicates that the oxidation peaks of these three species could not be separated at the bare electrode.

3.7. Individual electrocatalytic oxidation of dopamine, uric acid and paracetamol on the SiO_2/MWCNT/func/GCE electrode by differential pulse voltammetry

Fig. 8 shows the individual determination of (a) dopamine, (b) uric acid and (c) paracetamol by differential pulse voltammetry (DPV). DPV was used to determine dopamine, uric acid and paracetamol because this technique offers good resolution and higher sensitivity when compared to cyclic voltammetry. As expected, the intensity of the current of the anodic peaks for dopamine, uric acid and paracetamol increased with an increase in the analyte concentrations. This indicates that dopamine, uric acid and paracetamol were electrooxidized on the SiO_2/MWCNT/func/GCE electrode surface.

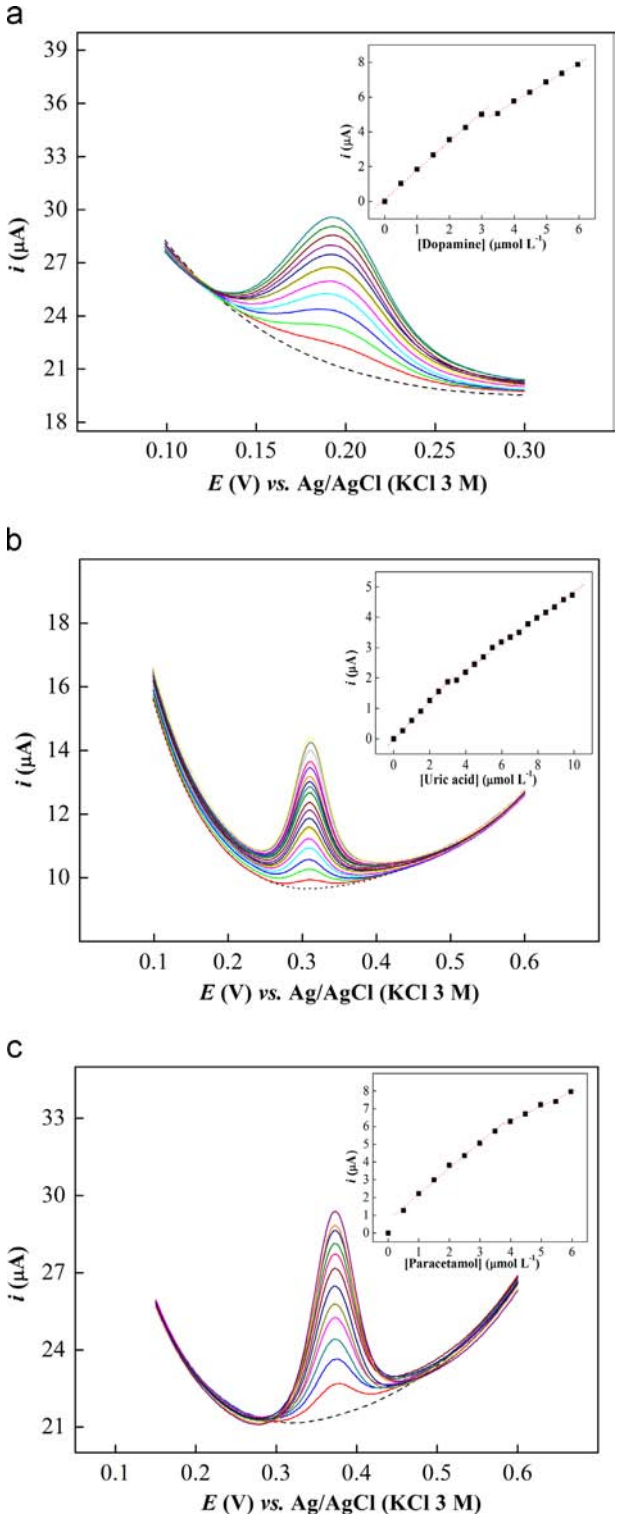

Fig. 8. Individual differential pulse voltammograms to SiO_2/MWCNT/func/GCE of (a) dopamine, (b) uric acid and (c) paracetamol with concentrations of dopamine ranging from 5.0×10^{-7} to 6.0×10^{-6} mol L^{-1}, and concentrations of uric acid and paracetamol ranging of 5.0×10^{-7}–1.0×10^{-5} mol L^{-1} and 5.0×10^{-7}–6.0×10^{-6} mol L^{-1}, respectively, in PBS, pH 7.0. Inset figures: Plots of current intensities against concentration of dopamine, uric acid and paracetamol.

The analytical curve for current (i) versus [dopamine] (inset Fig. 8a) indicated two linear relationships in the concentration range of 5.0×10^{-7} to 6.0×10^{-6} mol L^{-1}, with a linear correlation of $r=0.999$, $n=7$, according to the following equation: $i(A)=1.3958 \times 10^{-7}+1.66$ [dopamine]/μmol L^{-1} and $i(A)=1.2476 \times 10^{-8}+1.11$[dopamine]/μmol L^{-1} with a linear correlation of $r=0.998$, $n=6$. The decreased slope (sensitivity) with increasing DA concentration was due to kinetic limitations [58] and may be explained as follows: with an increase in the DA concentration, the irreversible adsorption of the reagent/product on the electrode surface hinders further oxidation of DA on the electrode surface [59].

Similarly, the analytical curves current (i) × [uric acid] (inset Fig. 8b) and (i) × [paracetamol] (inset Fig. 8c) also showed two good linear relations in the concentration range of 5.0×10^{-7}–1.0×10^{-5} mol L^{-1} and 5.0×10^{-7}–6.0×10^{-6} mol L^{-1}, respectively. Uric acid had correlation coefficients of $r=0.999$, $n=7$, and $r=0.998$, $n=13$, respectively, according to the following equation: $i(A)=2.731 \times 10^{-8}+0.635$ [uric acid]/μmol L^{-1} and: $i(A)=5.289 \times 10^{-7}+0.431$ [uric acid]/μmol L^{-1}. Paracetamol had correlations coefficients of $r=0.997$, $n=7$, and $r=0.992$, $n=5$, respectively, according to the following equation: $i(A)=7.109 \times 10^{-7}+1.468$ [paracetamol]/μmol L^{-1} and: $i(A)=3.071 \times 10^{-8}+0.814$ [paracetamol]/μmol L^{-1}. The decreased slopes with increasing UA and PAR concentrations occurred in a similar fashion as with dopamine (DA). The limits of detection of dopamine, uric acid and paracetamol were individually calculated using statistical methods [60] as 0.014, 0.068 and 0.098 μmol L^{-1}, respectively.

The SiO_2/MWCNT/func/GCE electrode showed an excellent electrocatalytic response to individual determinations of dopamine, uric acid and paracetamol at potentials of 0.189, 0.31 and 0.372 V, respectively. As can be seen, the SiO_2/MWCNT/func/GCE electrode showed good peak separation of dopamine and uric acid with a difference of 121 mV and also showed good peak separation of uric acid and paracetamol with a difference of 62 mV. This electrode could, therefore, be used for the simultaneous determination of dopamine, uric acid and paracetamol.

3.8. Determination of a mixture of dopamine, uric acid and paracetamol using the SiO_2/MWCNT/func/GCE electrode by differential pulse voltammetry

Taking into account the good peak separation between dopamine, uric acid and paracetamol in individual determinations, a study was performed to test the versatility of the SiO_2/MWCNT/func/GCE electrode for the selective determination of a mixture of dopamine, uric acid and paracetamol. DPV was carried out in the mixture by changing the concentration of one species and maintaining those of the other two species constant.

Fig. 9a shows the determination of dopamine, keeping the concentrations of uric acid and paracetamol constant at 9.9×10^{-6} mol L^{-1}. As can be seen, the oxidation peak current intensities increased linearly with an increase in the concentration of dopamine in the range of 1.6×10^{-5}–1.9×10^{-4} mol L^{-1}. This indicates that the SiO_2/MWCNT/func/GCE electrode presents an excellent response to the electrooxidation of dopamine in the presence of uric acid and paracetamol. The inset in Fig. 9a shows the analytical curve of current (i) versus [dopamine] in the presence of uric acid and paracetamol. The curve presented a good linear relation in the concentration range of 1.6×10^{-5}–1.9×10^{-4} mol L^{-1}, with a linear correlation coefficient of $r=0.997$, $n=6$ and $r=0.997$, $n=6$, respectively, according to the following equation: $i(A)=8.048 \times 10^{-7}+0.268$ [dopamine]/μmol L^{-1} and: $i(A)=1.154 \times 10^{-6}+0.115$ [dopamine]/μmol L^{-1}. The peak currents of UA and PAR decreased slightly depending on the cycle number without a significant loss of electrocatalytic activity, similar to what occurs with other modified electrodes [61–64]. These occur

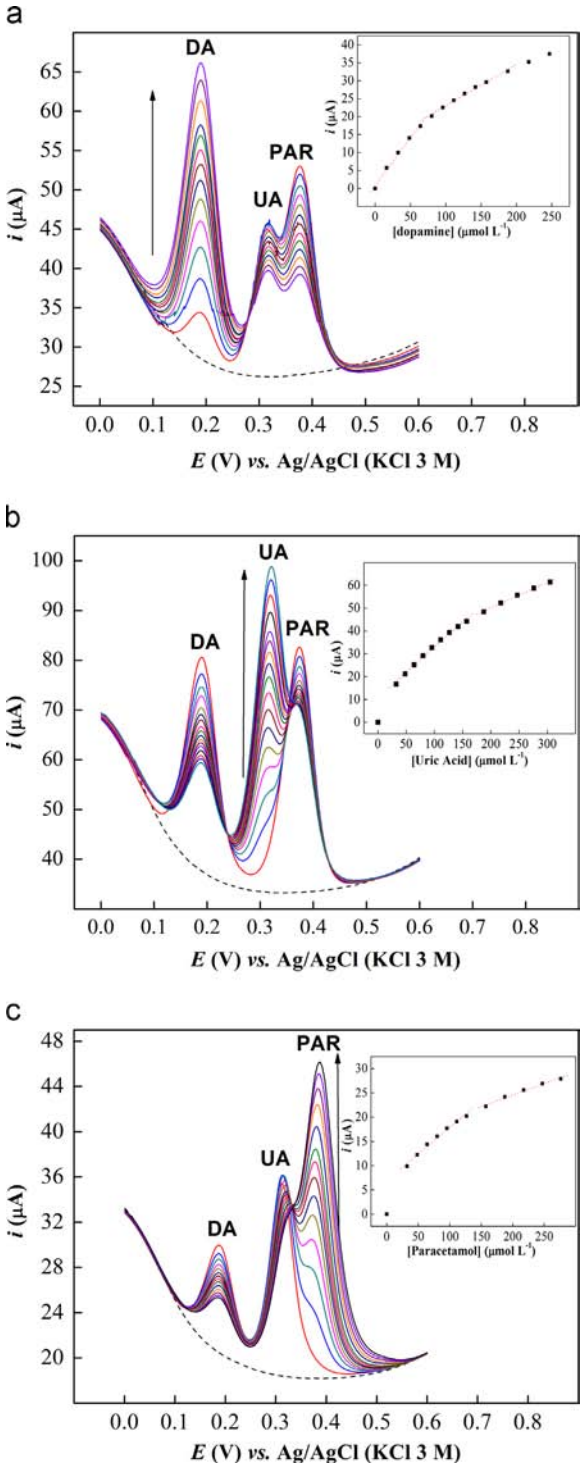

Fig. 9. (a) Differential pulse voltammograms the SiO_2/MWCNT/func/GCE electrode for dopamine at concentrations ranging from 1.62×10^{-5} to 1.9×10^{-4} mol L^{-1}, in the presence of uric acid and paracetamol at 9.9×10^{-6} mol L^{-1}, in PBS, pH 7.0. Inset figure: Plot of current intensity against the concentration of dopamine for (b) uric acid at concentrations ranging from 1.6×10^{-5} to 3.05×10^{-4} mol L^{-1}, in the presence of dopamine and paracetamol at 9.9×10^{-6} mol L^{-1}. Inset figure: Plot of current intensity against the concentration of uric acid and (c) paracetamol with concentrations ranging from 1.6×10^{-5} to 2.8×10^{-4} mol L^{-1}, in the presence of dopamine at 4.97×10^{-6} mol L^{-1} and uric acid at 1.5×10^{-5} mol L^{-1}, in PBS, pH 7.0. Inset figure: Plot of current intensity against the concentration of paracetamol.

since, with an increased DA concentration, the irreversible adsorption of the reagent/product on the electrode surface hinders the further oxidation of uric acid and paracetamol on the electrode surface. Similarly, the study was performed for the determination of uric acid,

keeping the concentrations of dopamine and paracetamol constant at 9.9×10^{-6} mol L^{-1}, and for the determination of paracetamol, keeping the concentrations of dopamine constant at 4.97×10^{-6} mol L^{-1} and uric acid constant at 1.5×10^{-5} mol L^{-1} as shown in Fig. 9b and c, respectively. It can be seen that the anodic peak current intensities also increased with an increase in the uric acid concentration ranging from 1.62×10^{-5} to 3.05×10^{-4} mol L^{-1} and paracetamol concentration ranging from 1.62×10^{-5} to 2.8×10^{-4} mol L^{-1}. The insets in Fig. 9b and c indicate that the analytical curves of currents (i) versus [uric acid] and (i) versus [paracetamol], respectively, showed a good linear relationship with the concentrations studied, with linear correlation coefficients $r=0.997$, $n=9$ and $r=0.998$, $n=5$, respectively, according to the following equation: $i(A)=1.077 \times 10^{-5}$ +0.221 [uric acid]/μmol L^{-1} and: $i(A)=2.79 \times 10^{-5}$+0.111 [uric acid]/μmol L^{-1}. Paracetamol had correlations coefficients of $r=0.997$, $n=7$, and $r=0.992$, $n=5$, respectively, according to the following equation: $i(A)=6.95 \times 10^{-8}$+0.109 [paracetamol]/μmol L^{-1} and: $i(A)=1.503 \times 10^{-6}$+0.048 [paracetamol]/μmol L^{-1}. Similarly, in the DA determination, the peak currents of species that were kept constant decreased slightly depending on the cycle number due to adsorption of the species on the electrode surface without a significant loss of electrocatalytic activity.

Considering the studies performed above, the good electrocatalytic response shown by the SiO_2/MWCNT/func/GCE electrode for the determination of a mixture of dopamine, uric acid and paracetamol in pH 7.0 allows this electrode to be used in the simultaneous determination of these compounds.

3.9. Simultaneous determination of dopamine, uric acid and paracetamol

Fig. 10a shows the simultaneous determination of dopamine (DA), uric acid (UA) and paracetamol (PAR) by the SiO_2/MWCNT/func/GCE electrode in PBS buffer, pH 7.0. The oxidation peak currents for (DA), (UA) and (PAR) increased proportionally with the concentration of dopamine ranging from 1.33×10^{-7} to 4.64×10^{-6} mol L^{-1} and concentrations of uric acid and paracetamol ranging from 6.7×10^{-7} to 4.65×10^{-6} mol L^{-1}, indicating that the SiO_2/MWCNT/func/GCE electrode can be used for the simultaneous determination of dopamine, uric acid and paracetamol without any interference. Fig. 10b shows the analytical curves of current (i) versus [dopamine], (i) versus [uric acid] and (i) versus [paracetamol]. As can be seen, the anodic peak currents were linearly proportional to the concentration of dopamine, uric acid and paracetamol. This can be expressed by the linear equations: $i(A)=3.62 \times 10^{-6}$+1.30102 [dopamine]/μmol L^{-1}, with $r=0.998$, $n=7$, $i(A)=5.045 \times 10^{-6}$+0.6054 [uric acid]/μmol L^{-1}, with $r=0.998$, $n=7$ and $i(A)=2.426 \times 10^{-6}$+1.2384 [paracetamol]/μmol L^{-1}, with $r=0.998$, $n=10$. As can be seen, the values of the slopes of dopamine, uric acid and paracetamol obtained in the simultaneous determination are quite similar compared to individual determinations of these species. This indicates that dopamine, uric acid and paracetamol did not significantly interfere with each other during their identification and simultaneous determination.

3.10. Interference study and urine sample analysis

The effect of interfering species commonly found in biological samples in the determination of dopamine, uric acid and paracetamol, such as NADH and ascorbic acid (AA), on the analytical response of the SiO_2/MWCNT/func/GCE electrode was studied. NADH and AA showed no signal in the potential range studied and did not affect the determination of dopamine, uric acid and paracetamol. This behavior could be explained by negative charges of ascorbic acid and NADH at pH 7.0 and that Nafion, together with the presence of $-COO^-$ groups following acid treatment of the SiO_2/MWCNT material, acts as an anion barrier, which can prevent the electro-oxidation of AA and NADH [64,65].

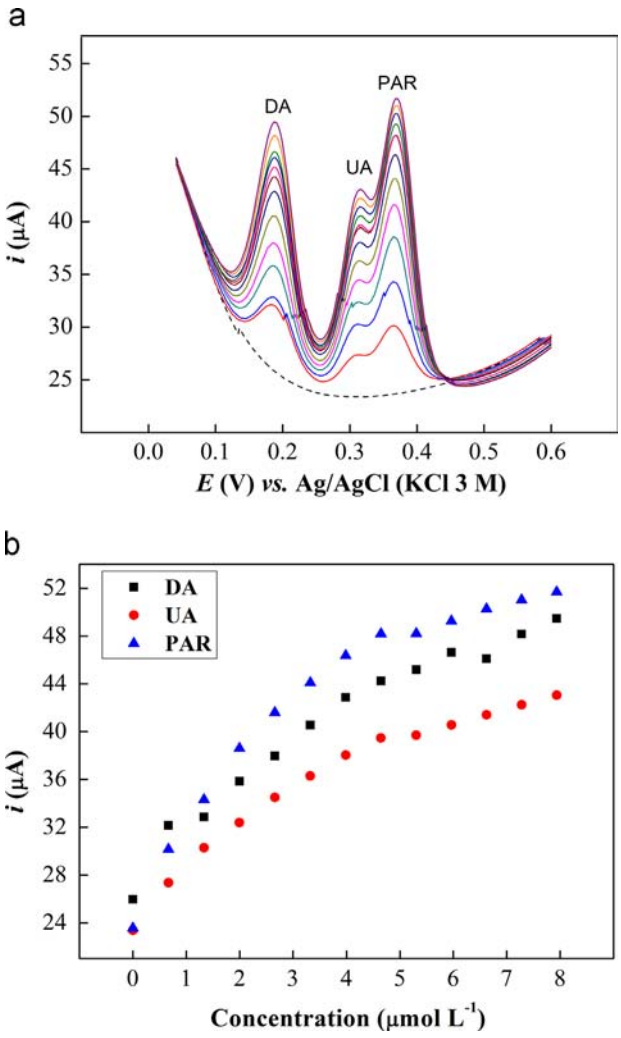

Fig. 10. (a) Simultaneous determination of dopamine (DA), uric acid (AU) and paracetamol (PAR) at the SiO_2/MWCNT/func/GCE electrode. Differential pulse voltammograms performed with different concentrations of dopamine, uric acid and paracetamol. Dopamine concentrations ranged from 1.33×10^{-6} to 4.64×10^{-6} mol L^{-1} and concentrations of uric acid and paracetamol ranged from 6.7×10^{-7} to 4.65×10^{-6} mol L^{-1}, in PBS, pH 7.0. (b) Analytical curve of the SiO_2/MWCNT/func/GCE electrode for dopamine (DA), uric acid (AU) and paracetamol (PAR). Measurements performed with different concentrations of dopamine, uric acid and paracetamol from 1.33×10^{-6} to 4.65×10^{-6} mol L^{-1}.

The utilization of the SiO_2/MWCNT/func/GCE electrode in real sample analysis was investigated. The urine sample was obtained from a healthy volunteer. The DPV results of urine samples were obtained for dopamine, uric acid and paracetamol in PBS solution to which aliquots of 10 μL of a urine stock solution were consecutively added to the electrochemical cell without any pretreatment process. The urine sample showed only an oxidation peak at 0.31 V for uric acid (Fig. 11). To confirm SiO_2/MWCNT/func/GCE electrode performance with regard to the determination of dopamine, uric acid and paracetamol in urine, the electrochemical cell was spiked with known concentrations of DA and PAR prepared by adding known amounts of the two compounds to the urine (inset Fig. 11). It was observed that all peak currents showed a direct relationship with the dopamine, uric acid and paracetamol concentrations present in urine. The amount of dopamine, uric acid and paracetamol in human urine samples was determined by the calibration method using DPV; the results are summarized in Table 3.

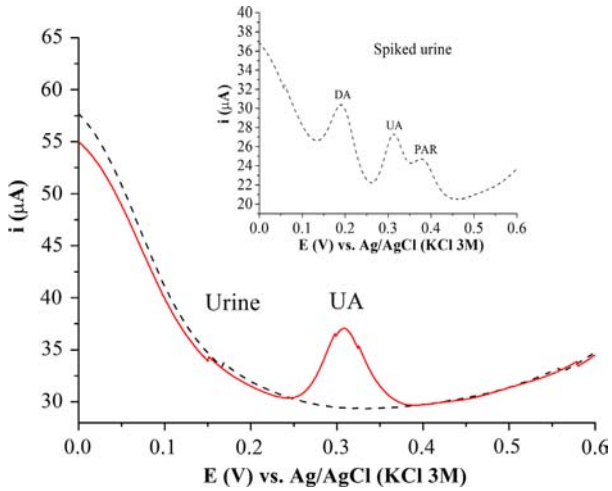

Fig. 11. Differential pulse voltammograms of the SiO_2/MWCNT/func/GCE electrode for a urine sample obtained in PBS solution, pH 7.0. Inset figure: Differential pulse voltammograms spiked urine of dopamine and paracetamol.

Table 3
Recovery results for dopamine, uric acid and paracetamol in urine samples.

Urine sample	Added (μmol L^{-1})	Found (μmol L^{-1})	Recovery %
Dopamine	0.049	0.046	93.8
Uric acid	–	1.11	–
Paracetamol	0.05	0.049	98

Average of five determinations.

The detection limits were calculated for dopamine, uric acid and paracetamol in urine using statistical methods and compared with the values obtained in PBS solution. The similarity of the values obtained for DA (PBS solution = 0.014 μmol L^{-1} and urine sample = 0.11 μmol L^{-1}), UA (PBS solution = 0.068 μmol L^{-1} and urine sample = 0.026 μmol L^{-1}) and PAR (PBS solution = 0.098 μmol L^{-1} and urine sample = 0.056 μmol L^{-1}) suggests that the proposed SiO_2/MWCNT/func/GCE electrode can be used to determine the concentration of dopamine, uric acid and paracetamol in real samples. The low detection limit shown for the SiO_2/MWCNT/func/GCE electrode can be explained by the mesoporous structure of the material, facilitating the mass transfer of dopamine, uric acid and paracetamol. The reproducibility of the preparation of the SiO_2/MWCNT/func/GCE electrode was very good with an accuracy of 100%. The reproducibility of the sensor was tested by detecting the DPV response of 5.0 μmol L^{-1} DA, UA and PAR individually in PBS (pH 7.0) with the same electrode ten times and with five different sensors prepared at room temperature under the same conditions. The SiO_2/MWCNT/func/GCE electrode presented convincing repeatability without significant loss of electrocatalytic activity with a relative standard deviation (RSD) that was minor (5%) for all species.

Table 4 shows the efficiency of the SiO_2/MWCNT/func/GCE electrode for dopamine, uric acid and paracetamol determinations compared with other electrodes modified with carbon nanotubes at pH 7.0. This electrode has a lower limit of detection for the determination of dopamine, uric acid and paracetamol in comparison with most modified materials.

4. Conclusions

A silica-based hybrid material containing carbon nanotubes, SiO_2/MWCNT, showed a heterogeneous distribution of pore size in the mesoporous region and nanotubes presented a good distribution in the silica matrix. Films of the hybrid material formed on the surface of a glassy carbon electrode, SiO_2/MWCNT/func/GCE, resulted in a good electrocatalytic response regarding individual and simultaneous determination of dopamine, uric acid and acetaminophen with a low detection limit. This electrode also showed a good electrocatalytic response for these species in urine without any interference between them. Such characteristics, coupled with the robustness displayed by the modified electrodes, suggest that they are potentially useful in the determination of these species in real samples.

Table 4
Efficiency of the SiO_2/MWCNT/func/GCE electrode for dopamine, uric acid and paracetamol determination in pH 7.0, compared with previously reported modified electrodes.

Modified materials	Detection limit	Potential
	(μmol L^{-1})	DA, UA, PAR
SiO_2/MWCNTs (This work)	0.014 (DA)	0.189 V DA
	0.068 (UA)	0.31 V UA
	0.098 (PAR)	0.37 V PAR vs. Ag/AgCl
DMS/$(ensal)_2$Cu [66]	0.52 (DA)	−0.02 V DA vs. SCE
	–	–
	–	–
MWCNT/CCE sol–gel [67]	0.22 (DA)	0.21 V DA
	–	–
	0.12 (PAR)	0.39 V PAR vs. Ag/AgCl
PPy/GO composite film [68]	0.023	0.17 V DA
	–	–
	–	0.33 V UA vs. SCE
(HCNTs/GCE) [69]	0.8	0.089 V DA
	(DA)	0.183 V UA
	1.5	–
	(UA)	vs. SCE
SWCNTs/CPB multilayer films [70]	0.6	0.208 V DA
	(DA)	0.332 V UA
	7.0	–
	(UA)	vs. SCE

Ag/AgCl vs. SCE = −0.045 V.
DMS/$(ensal)_2$Cu (disordered mesoporous silica chemically modified with ensal copper complexes); MWCNT/CCE sol–gel (uniform layer of SWCNT onto carbon–ceramic electrode); polypyrrole (PPy) and (GO) graphene thin films); HCNTs/GCE (helical carbon nanotubes modified glassy carbon electrode).

Acknowledgments

T.C.C. acknowledges FAPESP for post-doctoral fellowship grant 2011/23047-7. The authors are also grateful to FAPESP (2012/17689-9), CNPq and FAPERGS for financial support.

References

[1] M. Noroozifar, M. Khorasani-Motlagh, R. Akbari, M.B. Parizi, Biosens. Bioelectr. 28 (2011) 56–63.
[2] S. Komathi, A.I. Gopalan, K.P. Lee, Analyst 135 (2010) 397–404.
[3] L. Agui, P. Yanez-Sedeno, J.M. Pingarron, Anal. Chim. Acta 622 (2008) 11–47.
[4] J. Wang, Analyst 130 (2005) 421–426.
[5] K. Pyrzynska, Chemosphere 83 (2011) 1407–1413.
[6] A. Walcarius, Anal. Bioanal. Chem. 396 (2010) 261–272.
[7] A. Walcarius, A. Kuhn, Trends Anal. Chem. 27 (2008) 593–603.
[8] A. Walcarius, D. Mandler, J.A. Cox, M. Collinson, O. Lev, J. Mater. Chem. 15 (2005) 3663–3689.
[9] M.M. Collinson, Trends Anal. Chem. 21 (2002) 31–39.
[10] P.K. Jal, S. Patel, B.K. Mishra, Talanta 62 (2004) 1005–1028.
[11] K.S.W. Sing, D. Everett, R.A.W. Haul, L. Moscou, R.A. Pierotti, J. Rouquerol, T. Siemieniewska, Pure Appl. Chem. 57 (1985) 603–619.
[12] B.J. Melde, B.J. Johnson, P.T. Charles, Sensors 8 (2008) 5202–5228.
[13] B.G. Trewyn, S. Giri, I.I. Slowing, V.S.Y. Lin, Chem. Commun. 31 (2007) 3236–3245.
[14] Y. Battie, O. Ducloux, L. Patout, P. Thobois, A. Loiseau, Sens. Actuators, B 163 (2012) 121–127.
[15] J. Lin, Z. Wei, H. Zhang, M. Shao, Biosens. Bioelectr. 41 (2013) 342–347.
[16] A.H. Lu, W. Schmidt, S.D. Tatar, B. Spliethoff, J. Popp, W. Kiefer, F. Schüth, Carbon 43 (2005) 1811–1814.
[17] D. Ragupathy, A.I. Gopalan, K-P. Lee, Sens. Actuators, B 143 (2010) 696–703.

[18] K. Balasubramanian, M. Burghard, Small 1 (2005) 180–192.
[19] E. Colín-Orozco, M.T. Ramírez-Silva, S. Corona-Avendano, M. Romero-Romo, M. Palomar-Pardavé, Electrochim. Acta 85 (2012) 307–313.
[20] S. Thiagarajan, S. Chen, Talanta 74 (2007) 212–222.
[21] R.M. Wightman, Anal. Chem. 60 (1988) 769A–779A.
[22] J.W. Mo, B. Ogorevc, Anal. Chem. 73 (2001) 1196–1202.
[23] D. Lakshmi, M.J. Whitcombe, F. Davis, P.S. Sharma, B.B. Prasad, Electroanalysis 23 (2011) 305–320.
[24] C. Wang, R. Yuan, Y. Chai, S. Chen, Y. Zhang, F. Hu, M. Zhang., Electrochim. Acta 62 (2012) 109–115.
[25] H. Beitollahi, J-B. Raoof, R. Hosseinzadeh, Talanta 85 (2011) 2128–2134.
[26] R.N. Goyal, V.K. Gupta, S. Chatterjee, Sens. Actuators, B 149 (2010) 252–258.
[27] S. Parrot, P.-C. Neuzeret, L. Denoroy, J. Chromatogr. B 879 (2011) 3871–3878.
[28] R. Kandár, P. Drábková, R. Hampl, J. Chromatogr. B 879 (2011) 2834–2839.
[29] R. López-Serna, M. Petrovic, D. Barceló, J. Chromatogr. A 1252 (2012) 115–129.
[30] M.R. Moghadam, S. Dadfarnia, A.M.H. Shabani, P. Shahbazikhah, Anal. Biochem. 410 (2011) 289–295.
[31] M.R. Khoshayand, H. Abdollahi, M. Shariatpanahi, A. Saadatfard, A. Mohammadi, Acta. Part A 70 (2008) 491–499.
[32] H. Huang, Y. Gao, F. Shi, G. Wang, S.M. Shah, X. Su, Analyst 137 (2012) 1481–1486.
[33] J. Yang, M. Hu, Y. Cai, J. Tang, H. Li, J. Sep. Sci. 33 (2010) 3710–3716.
[34] L. Li, Y. Lu, Y. Ding, Y. Cheng, W. Xu, F. Zhang., J. Fluoresc. 22 (2012) 591–596.
[35] Y. Yue, G. Hu, M. Zheng, Y. Guo, J. Cao, S. Shao, Carbon 50 (2012) 107–114.
[36] Y. Fan, J.-H. Liu, H.-T. Lu, Q. Zhang, Colloids Surf., B 85 (2011) 289–292.
[37] Z. Wang, M. Shoji, H. Ogata, Analyst 136 (2011) 4903–4905.
[38] M. Mallesha, R. Manjunatha, C. Nethravathi, G.S. Suresh, M. Rajamathi, J. S. Melo, T.V. Venkatesha, Bioelectrochemistry 81 (2011) 104–108.
[39] Y.-C. Chiang, W.-H. Lin, Y.-C. Chang, Appl. Surf. Sci. 257 (2011) 2401–2410.
[40] D.A. Shirley, Phys. Rev. B: Condens. Matter 5 (1972) 4709–4714.
[41] E.V. Benvenutti, C.C. Moro, T.M.H. Costa, M.R. Gallas, Quim. Nova 32 (2009) 1926–1933.
[42] S. Lowell, J.E. Shields, M. Thomas, A.M. Thommes, Characterization of Porous Solids and Powders: Surface Area Pore Size and Density, ed, Springer, Netherlands, 2006.
[43] E. Reale, A. Leyva, A. Corma, C. Martínez, H. García, F. Rey, J. Mater. Chem. 15 (2005) 1742–1754.
[44] Z. Deng, B. Peng, D. Chen, F. TangA.J. Muscat, Langmuir 24 (2008) 11089–11095.
[45] U.K.H. Bangi, M.S. Kavale, S. Baek, H.-H. Park, J. Sol–Gel Sci. Technol. 62 (2012) 201–207.
[46] A.F. Holloway, G.G. Wildgoose, R.G. Compton, L. Shao, M.L.H. Green, J. Solid State Electrochem. 12 (2008) 1337–1348.
[47] A.J. Paula, D. Stéfani, A.G.S. Filho, Y.A. Kim, M. Endo, O.L. Alves, Chem. Eur. J. 17 (2011) 3228–3237.
[48] C. Huiqun, Z. Meifang, L. Yaogang, J. Solid State Chem. 179 (2006) 1208–1213.
[49] F.C. Moraes, M.F. Cabral, L.H. Mascaro, S.A.S. Machado, Surf. Sci. 605 (2011) 435–440.
[50] A.G.S. Filho, A. Jorio, G. Samsonidze, G. Dresselhaus, R. Saito, M.S. Dresselhaus, Nanotechnology 14 (2003) 1130–1139.
[51] P.T. Araujo, M.M.S. TerronesDresselhaus, Mater. Today 15 (2012) 98–109.
[52] M.T. Martínez, M.A. Callejas, A.M. Benito, M. Cochet, T. Seeger, A. Ansón, J. Schreiber, C. Gordon, C. Marhic, O. Chauvet, J.L.G. Fierro, W.K. Maser, Carbon 41 (2003) 2247–2256.
[53] M.S. Dresselhaus, G. Dresselhaus, R. Saito, A. Jorio, Phys. Reports 409 (2005) 47–99.
[54] S. Kundu, Y. Wang, W. Xia, M. Muhler, J. Phys. Chem. C 112 (2008) 16869–16878.
[55] J.-H. Zhou, Z.-J. Sui, J. Zhu, P. Li, D. Chen, Y.-C. Dai, W.-K. Yuan, Carbon 45 (2007) 785–796.
[56] Y.-C. Chiang, W.-H. Lin, Y.-C. Chang, Appl. Surf. Sci. 257 (2011) 2401–2414.
[57] J.H. Kim, M.-J. Song, C. Lee, J.J.-H. Lee, J.-H. Kim, N.K. Min, Carbon 52 (2013) 398–407.
[58] M. Mazloum-Ardakani, H. Beitollahi, B. Ganjipour, H. Naeimi, M. Nejati, Biolectrochemistry 75 (2009) 1–8.
[59] H.-S. Wang, T.-H. Li, W.-L. Jia, H.-Y. Xu, Biosens. Bioelectr. 22 (2006) 664–669.
[60] O.B. da Silva, S.A.S. Machado, Anal. Methods 4 (2012) 2348–2354.
[61] B. Zhang, D. Huang, X. Xu, G. Alemu, Y. Zhang, F. Zhan, Y. Shen, M. Wang, Electrochim. Acta 91 (2013) 261–266.
[62] Z. Dursun, B. Gelmez, Electroanalysis 22 (2010) 1106–1114.
[63] M. Noroozifar, M. Khorasani-Motlagh, R. Akbari, M.B. Parizi, Biosens. Bioelectr. 28 (2011) 56–63.
[64] P.-Y. Chen, R. Vittal, P.-C. Niena, K.-C. Ho., Biosens. Bioelectr. 24 (2009) 3504–3509.
[65] Z.A. Alothman, N. Bukhari, S.M. Wabaidur, S. Haider, Sens Actuators, B 146 (2010) 314–320.
[66] M.P. dos Santos, A. Rahim, N. Fattori, L.T. Kubota, Y. Gushikem, Sens. Actuators, B 171–172 (2012) 712–718.
[67] B. Habibi, M. Jahanbakhshi, M.H. Pournaghi-Azar, Electrochim. Acta 56 (2011) 2888–2894.
[68] P. Si, H. Chen, P. Kannan, D-H. Kim, Analyst 136 (2011) 5134–5138.
[69] R. Cui, X. Wang, G. Zhang, C. Wang, Sens. Actuators, B 161 (2012) 1139–1143.
[70] Y. Zhang, Y. Pan, S. Su, L. Zhang, S. Li, M. Shao, Electroanalysis 19 (2007) 1695–1701.